arXiv:1108.5978v1 [cond-mat.other] 30 Aug 2011

Asymptotic motion of a single vortex in a rotating semi-infinite cylinder

J.M. Karimäki*,†, R. Hänninen*, and E.V. Thuneberg†
*Low Temperature Laboratory, Aalto University, P.O. Box 15100, FI-00076 AALTO, Finland and
†Department of Physical Sciences, University of Oulu, Oulu, Finland

(Dated: August 31, 2011)

We study numerically the behavior of a single quantized vortex in a rotating semi-infinite cylinder. We study in particular the spiraling motion of a vortex in a cylinder that is parallel to the rotation axis. We determine the asymptotic form of the vortex and its axial and azimuthal propagation velocities under a wide range of parameters. We also study the stability of the vortex line and the effect of tilting the cylinder from the rotation axis.

I. INTRODUCTION

Turbulence is a much studied, but not yet fully understood, phenomenon in both classical and quantum fluids. It is hoped that research in quantum turbulence will also shed light on classical turbulence, besides being an interesting field of research in itself[1,2]. To study quantum turbulence one needs to study the motion of quantized vortices. This has been done using various experimental and theoretical approaches[1,3–5]. In theoretical approaches the emphasis has been shifting to numerical simulations. Many of these include a large number of vortices and require a considerable amount of computing power, especially when calculations are performed using the full Biot-Savart equations[6]. However, there is still a need to better understand the motion of a single vortex. Since the motion of a curved vortex line is somewhat counter-intuitive, and solving the equations analytically is difficult and prone to errors, it is convenient to use numerical simulations. For single vortices, it also becomes a realistic possibility to scan a large volume of parameter space, i.e. various combinations of pressure p, temperature T, rotational velocity Ω, vessel size and shape, and initial vortex configurations.

An existing computer software, previously used mainly for studying the large scale behavior of many vortices[3,7,8], is applied to study the motion of a single vortex line. More specifically, we study the motion of a single superfluid vortex filament in a rotating semi-infinite cylinder, as illustrated in Figs. 1 and 2. Earlier studies by other researchers have considered a single vortex in a cylinder attached to a wire[9,10].

We assume the normal component of the velocity to be in solid-body rotation. Our main point of interest is the asymptotic velocity of the vortex end touching the side wall of the cylinder. We calculate the evolution of the vortex from the initial state using the vortex filament model of the two-fluid paradigm with Biot-Savart formalism, until the asymptotic situation is reached. Although we have used ^{3}He-B-specific parameters in our calculations, the methods and the results can be generalized to vortices in other superfluids and Bose-Einstein condensates in many cases.

One surprising effect discovered in our calculations is the stability of the vortex, even in the low temperature limit. This contradicts the expectations based on some earlier simulations and experimental results in ^{3}He-B[11–14]. We assume that the discrepancy with experiments is caused by some surface effects not accounted for in our model (such as pinning), or due to some uncontrolled heat leaks or superflows in the experiments that may destabilize the vortices.

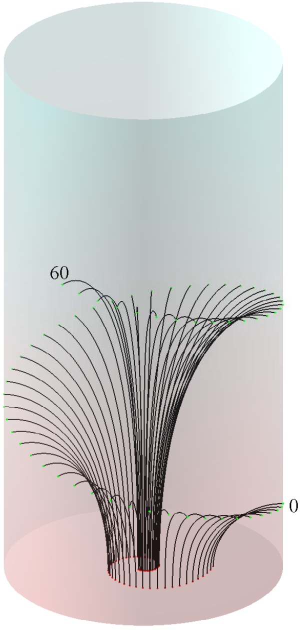

FIG. 1: The evolution of a vortex in a rotating coordinate system. The total time span $2.79/\alpha\Omega$ comprises 61 snapshots. Other parameters are $\mathrm{Re}_\alpha = 3.63$ ($\sim 0.4T_c$ in ^{3}He-B) and $\Omega R^2/\kappa = 13.6$.

II. THE MODEL

We study a superfluid in a half-infinite cylinder of radius R that rotates at constant angular velocity $\mathbf{\Omega}$. The axis of the cylinder may be tilted by an angle θ relative to the rotation axis. We use cylindrical coordinates (r, ϕ, z) fixed to the cylinder. Our study is based on the two-fluid model, where the normal and superfluid components have velocities $\mathbf{v}_\mathrm{n}$ and $\mathbf{v}_\mathrm{s}$, respectively. The normal component is assumed to be in rigid body rotation, $\mathbf{v}_\mathrm{n} = \mathbf{\Omega} \times \mathbf{r}$. This is a good assumption in ^{3}He-B, because mutual friction is weak in comparison to the viscosity of the normal fluid[15].

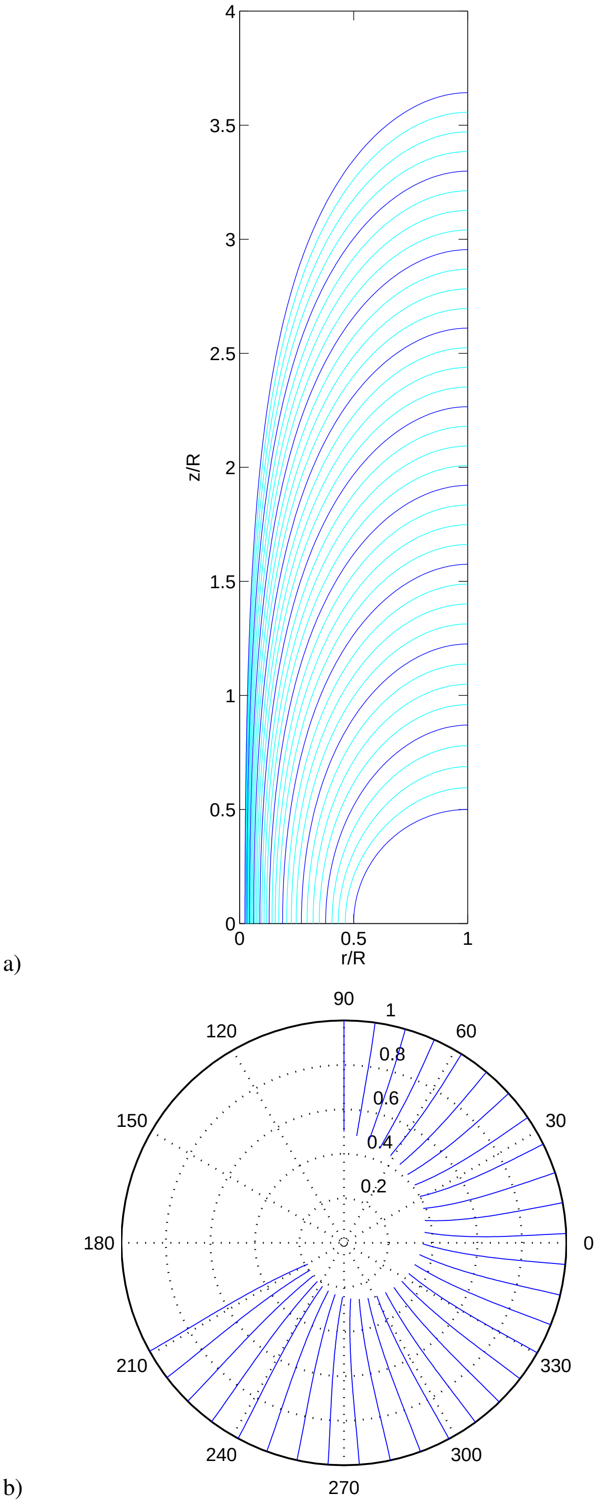

FIG. 2: The evolution of the vortex shown in Fig. 1 presented in cylindrical coordinates fixed to the rotating frame. a) (r, z) plot with 37 snapshots in time span $4.19/\alpha\Omega$. b) Polar plot with 31 snapshots in time span $1.40/\alpha\Omega$.

The superfluid velocity $\mathbf{v}_\mathrm{s}$ is determined by vortex lines[6]. The location of the vortex lines are given by $\mathbf{s}(\xi, t)$, which is parametrized by the vortex length ξ and time t. Partial derivatives with respect to ξ are denoted by primes. Then, the unit tangent of the vortex core line is the first derivative of $\mathbf{s}$ with respect to ξ. This is denoted by $\mathbf{s}'$ (or $\hat{\mathbf{s}}'$ to emphasize that it is a unit vector). The superfluid velocity $\mathbf{v}_\mathrm{s}$ is calculated using the (full) Biot-Savart formalism:

$$\mathbf{v}_\mathrm{s}(\mathbf{r}, t) = \mathbf{v}_\omega + \mathbf{v}_\mathrm{b}, \tag{1}$$

with

$$\mathbf{v}_\omega = \frac{\kappa}{4\pi} \int_\mathcal{L} \frac{(\mathbf{s}_1 - \mathbf{r}) \times d\mathbf{s}_1}{|\mathbf{s}_1 - \mathbf{r}|^3}, \tag{2}$$

where $\mathcal{L}$ denotes all the vortex lines and κ is the circulation of the superfluid velocity around a vortex line; all the positions and velocities are in laboratory coordinates. The first term, $\mathbf{v}_\omega$, in (1) needs to be numerically calculated from the integral (2). It has a divergence on the vortex core, which has to be cut off at the vortex core radius a, see Refs. 6 and 16 for details. The second term, $\mathbf{v}_\mathrm{b}$, is the boundary field, or image velocity field, needed to prevent flow across the vessel boundary. The boundary field $\mathbf{v}_\mathrm{b}$ can be calculated from the Laplace equation, or by the method of image vortices. To calculate $\mathbf{v}_\mathrm{b}$ we use the method of approximate image vortices as in Ref. 16.

The derivative of $\mathbf{s}(\xi, t)$ with respect to time defines the vortex line velocity $\mathbf{v}_\mathrm{L}$ except that the component of $\mathbf{v}_\mathrm{L}$ parallel to the line is not defined. The equation of motion is commonly written in laboratory coordinates as[6]

$$\mathbf{v}_\mathrm{L} = \mathbf{v}_\mathrm{s} + \alpha\hat{\mathbf{s}}' \times (\mathbf{v}_\mathrm{n} - \mathbf{v}_\mathrm{s}) - \alpha'\hat{\mathbf{s}}' \times [\hat{\mathbf{s}}' \times (\mathbf{v}_\mathrm{n} - \mathbf{v}_\mathrm{s})]. \tag{3}$$

It contains the mutual friction parameters α and α'. These parameters for ^{3}He depend (dramatically) on temperature and (moderately) on pressure[17,18]. Whenever not explicitly specifying their values, we use their temperature dependent values for ^{3}He-B at the pressure of 29.34 bar.

Using the fact that the normal component is in rigid body motion ($\mathbf{v}_\mathrm{n} = \mathbf{\Omega} \times \mathbf{r}$), we can rewrite the equation of motion (3) in rotating coordinates (where $\mathbf{v}_\mathrm{n} = 0$) as:

$$\mathbf{v}_\mathrm{L} = \alpha(\mathrm{Re}_\alpha \mathbf{v}_\mathrm{s} - \hat{\mathbf{s}}' \times \mathbf{v}_\mathrm{s}). \tag{4}$$

Here we have defined $\mathrm{Re}_\alpha := (1 - \alpha')/\alpha$, which has some similarity with the Reynolds number defined in normal fluids. In ^{3}He-B the quantity $\mathrm{Re}_\alpha(T)$ decreases monotonically from ∞ to 0, when the temperature increases form 0 to T_c. From now on all velocities will be in rotating coordinates, unless explicitly stated otherwise.

We study in particular the velocity of the vortex end in the long-time limit ($t \to \infty$). For that we define v_{Lz} and $v_{L\phi}$ by writing in the rotating frame

$$\mathbf{v}_\mathrm{L} = v_{Lz}\hat{\mathbf{e}}_z + v_{L\phi}\hat{\mathbf{e}}_\phi. \tag{5}$$

Note that typically $v_{L\phi}$ and Ω have opposite signs: for a growing vortex, as in our case, $v_{L\phi} < 0$, if $\Omega > 0$.

It is also possible to define the climbing angle β of the vortex in the rotating frame by $\tan\beta = v_{Lz}/v_{L\phi}$. The climbing angle in the laboratory frame satisfies $\tan\beta = v_{Lz}/(v_{L\phi} + \Omega R)$.

III. SCALING PROPERTIES

The parameter space of the system (without considering the parameters describing the initial vortex configuration) consists of mutual friction parameters α and α', the vortex core radius a, the circulation quantum κ, the cylinder radius R, the angular velocity Ω, and for a tilted cylinder the tilting angle θ. The exploration of this parameter space is simplified by dimensional analysis. Let us, for example, study the asymptotic axial velocity v_{Lz} (5) of the vortex end in the absence of tilting, $\theta = 0$. According to dimensional analysis, the dimensionless velocity $v_{Lz}/\Omega R$ can only depend on dimensionless quantities appearing in the problem, which in this case are R/a, $\Omega R^2/\kappa$, α and α'. Thus the parameter space is four-dimensional. Using properties specific to the present problem, we show in the following that this space can further be reduced to three dimensions exactly and to two dimensions approximately.

Let us consider the evolution of a vortex state from a fixed initial configuration. We see from Eq. (4) that varying α but keeping Re_α constant has the effect of changing the time scale only. This means that the dimensionless time is $\alpha\Omega t$ and the dimensionless line velocity is $\mathbf{v}_\mathrm{L}/\alpha\Omega R$, but otherwise there is no dependence on α. (Note that the dimensionless superfluid velocity $\mathbf{v}_\mathrm{s}/\Omega R$ does not have α.) Since the asymptotic velocity is obtained in the limit $t \to \infty$, the dependence on $\alpha\Omega t$ drops out. Since the system is dissipative (for $\alpha \neq 0$), the same final state can be obtained by a variety of initial states, i.e. the details of the initial state are not important either. Thus we conclude that the asymptotic velocity has the form

$$v_{Lz} = \alpha\Omega R\, f\left(\frac{\Omega R^2}{\kappa}, \frac{R}{a}, \frac{1-\alpha'}{\alpha}\right) \tag{6}$$

with some function f. The same form applies to the azimuthal velocity $v_{L\phi}$. Note that this is valid only in the rotating frame; the laboratory frame azimuthal velocity $v_{L\phi} + \Omega R$ does not have the form (6). Because the parameter $\Omega R^2/\kappa$ appears repeatedly, we define a unitless rotational velocity:

$$\nu := \frac{\Omega R^2}{\kappa}. \tag{7}$$

We also remind that the last parameter in (6) has the shorthand $\mathrm{Re}_\alpha \equiv (1-\alpha')/\alpha$.

An approximate simplification is offered by the fact that $\mathbf{v}_\mathrm{L}$ has only a weak logarithmic dependence on R/a, see e.g., Refs. 19 and 20. Hence, different values of R/a have only a minor effect on the the results; this is demonstrated in Fig. 3. Because of this weak dependence, we have fixed $R/a = 1.77 \times 10^5$ in all other calculations in this paper except the ones presented in Fig. 7.

IV. ASYMPTOTIC VORTEX VELOCITY IN A NON-TILTED CYLINDER

The vortex evolution is solved by numerically integrating Eq. (4) forward in time in the rotating frame. We use a quarter vortex ring as our initial condition. The radius of the ring is half of the cylinder radius. The ring is situated so that the vortex starts from the bottom of the cylinder and ends at the cylinder wall. Both ends of the vortex are allowed to move freely. Any vortex end touching the wall is always normal to it. In principle, a vortex line may also form a closed loop, without touching the boundary at all. A vortex loop may be created when a vortex line reconnects with itself. If a vortex loop comes very close to the wall, it reconnects with it, i.e. snaps open, with the two vortex ends connecting to the wall orthogonally. The use of a quarter vortex ring as the initial condition is not necessary, but is convenient in our case. What matters is whether the required asymptotic evolution (if it exists) is reached from the initial condition or not, and a quarter ring is suitable in a large parameter range. However, if the temperature is low and the shape of the vortex is far from the asymptotic one, the vortex may oscillate a long time before reaching a stable form. For $\mathrm{Re}_\alpha \gtrsim 100$, even the quarter ring vortex leads to long-lasting oscillations in the vortex shape.

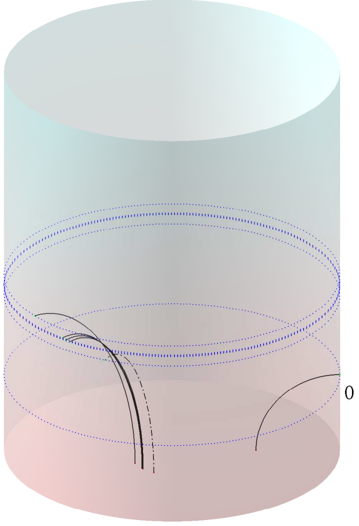

FIG. 3: The effect of the parameter R/a. The solid lines have R/a equal to 1, 2 and 4 times 1.77×10^5 while other parameters have constant values ($\alpha\Omega t = 0.75$, $\mathrm{Re}_\alpha = 3.63$ and $\nu = 13.6$). These can be contrasted to two cases, which differ by ±10% in the value of Ω from the middle case (the dashed line has $\alpha\Omega t = 0.82$ and $\nu = 15.0$ and the dash-dotted line has $\alpha\Omega t = 0.67$ and $\nu = 12.2$). The vortices are shown in the rotating coordinate system.

Our goal is to study the velocity of the end point of the vortex $\mathbf{v}_\mathrm{L}$ (5). Before going to the general case, we consider two limiting cases where analytic solutions are found.

In the limit $\nu \gg 1$, the cylinder wall at $r = R$ can be thought of as a plane and we suppose that the vortex line approaches the wall as a straight line normal to it[27]. We can now put $\mathbf{\Omega} = \Omega\hat{\mathbf{e}}_z$, $\mathbf{r} = R\hat{\mathbf{e}}_r$, a point on the large cylinder wall (or plane) and $\hat{\mathbf{s}}' = \hat{\mathbf{e}}_r$. This gives $\mathbf{v}_\mathrm{s} = -\Omega R\hat{\mathbf{e}}_\phi$ in rotating coordinates, and inserting it into (4) we get:

$$\mathbf{v}_\mathrm{L} = \Omega R\left[\alpha\hat{\mathbf{e}}_z + (\alpha'-1)\hat{\mathbf{e}}_\phi\right]. \tag{8}$$

Hence $v_{Lz} = \alpha\Omega R$, $v_{L\phi} = (\alpha'-1)\Omega R$, and $\tan\beta = -\mathrm{Re}_\alpha^{-1}$.

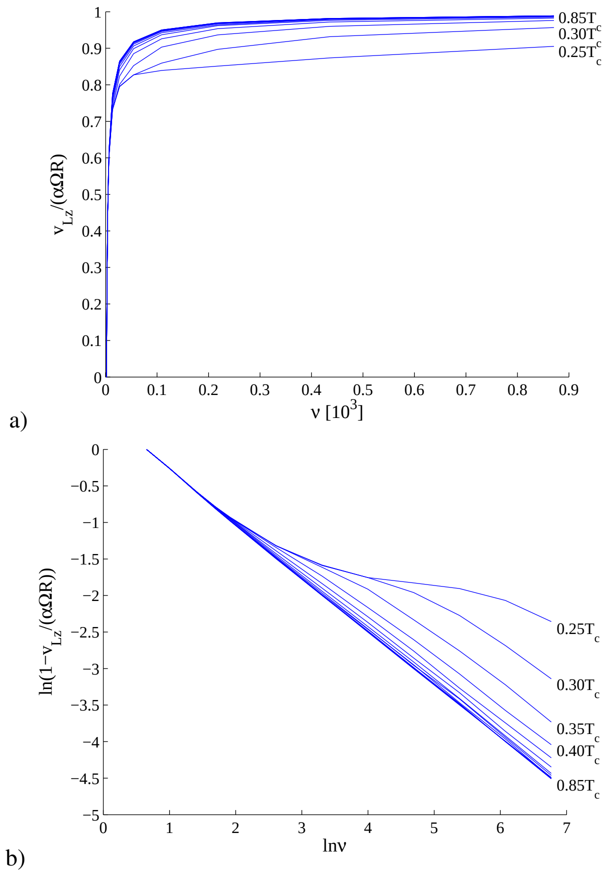

FIG. 4: The axial velocity of the vortex end v_{Lz}, plotted as a function of $\nu \equiv \Omega R^2/\kappa$ at Re_α values 78.6, 20.6, 7.65, 3.63, 2.18, 1.46, 1.03, 0.74, 0.53, 0.36, 0.24, 0.15, and 0.083, corresponding to temperatures $T/T_c = 0.25, 0.30, 0.35, ..., 0.85$ in ^{3}He-B, respectively. a) Plot in linear scale, b) Logarithmic plot.

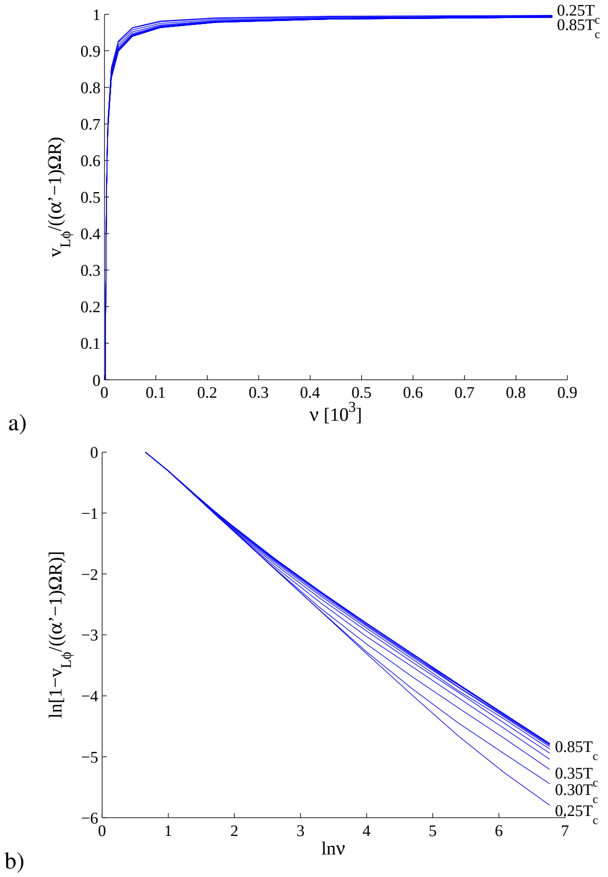

FIG. 5: The azimuthal velocity of the vortex end $v_{L\phi}$, plotted as a function of ν at the same values of the parameter Re_α as used in Fig. 4a and Fig. 4b, again corresponding to temperatures $T/T_c = 0.25, 0.30, 0.35, ..., 0.85$ in ^{3}He-B. a) Plot in linear scale, b) Logarithmic plot.

Another exact result corresponds to vanishing velocity, $\mathbf{v}_\mathrm{L} = 0$. This is obtained in the case that the one-vortex and no-vortex states are in equilibrium. This means that there is no force to drive the vortex and therefore the vortex end must be stationary in the rotating frame. The critical rotational velocity corresponding to this will be derived below, and is given in Eq. (16). In the dimensionless form it corresponds to $\nu_c \equiv \Omega_c R^2/\kappa = (1/2\pi)\ln(R/a)$, which in our case ($R/a = 1.77 \times 10^5$) has the value 1.92.

The numerically calculated v_{Lz} is depicted in Fig. 4a. It shows v_{Lz} as function of ν at different temperatures. The lowest point corresponds to ν_c, where v_{Lz} vanishes. For large ν the result tends to the analytic result (8). These two limits are obeyed at all temperatures, but a temperature dependence remains in between. For quantitative purposes it seems reasonable to write

$$v_{Lz} = \alpha\Omega R(1 - \epsilon_z). \tag{9}$$

where $\epsilon_z \to 0$ for $\nu \to \infty$. The value of ϵ_z defined hereby is shown as a function of ν as a log-log plot in Fig. 4b.

Figure 4b shows at low values of Re_α (or, equivalently, at high values of T/T_c) an almost perfect linear relationship between $\ln\epsilon_z$ and $\ln\nu$. In order to fit this, we keep the first (analytically obtained) point ($\nu = \nu_c, \epsilon_z = 0$) fixed:

$$\ln\epsilon_z \simeq k_z \ln\frac{\nu}{\nu_c}. \tag{10}$$

With $\mathrm{Re}_\alpha = 0.083$ ($\sim 0.85T_c$ in ^{3}He-B), fitting in the range $\nu \in [\nu_c, 871]$ gives $k_z \simeq -0.741$. Thus,

$$v_{Lz} \simeq \alpha\Omega R\left[1 - \left(\frac{\nu_c}{\nu}\right)^{0.741}\right]. \tag{11}$$

We now proceed to analyze the azimuthal velocity $v_{L\phi}$. The numerically calculated $v_{L\phi}$ is shown in Fig. 5a. Similarly as for v_{Lz}, in order to resolve more details we define ϵ_ϕ by

$$v_{L\phi} = (\alpha' - 1)\Omega R(1 - \epsilon_\phi). \tag{12}$$

The log-log plot of ϵ_ϕ vs. ν is shown in Fig. 5b.

We see that there is an approximately linear dependence of $\ln\epsilon_\phi$ on $\ln\nu$:

$$\ln\epsilon_\phi \simeq k_\phi \ln\frac{\nu}{\nu_0}. \tag{13}$$

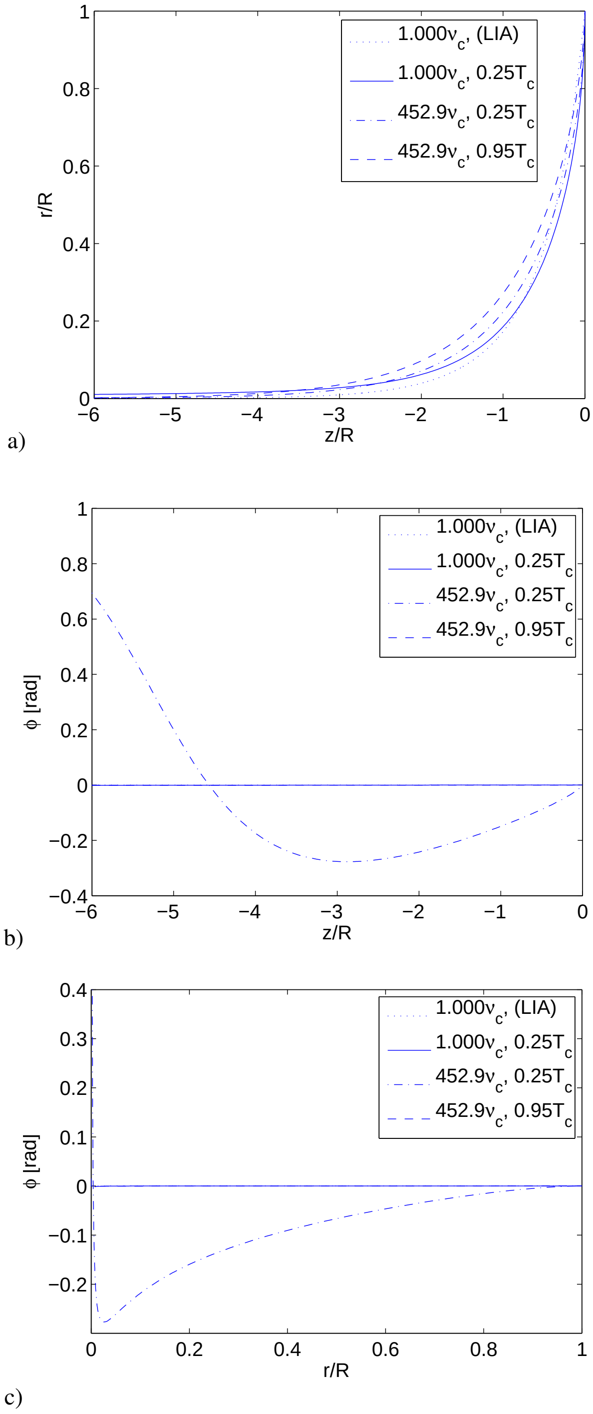

FIG. 6: Asymptotic vortex forms plotted for combinations of low and high temperatures ($0.25T_c$; $0.95T_c$) and rotational velocities (ν_c; $452.9\nu_c$): a) r against z, b) ϕ against z, c) ϕ against r. The vortex shape at $\nu = \nu_c$ is independent of temperature, so only the solution at $0.25T_c$ is plotted. Another point to make is the negligible variation of ϕ in all the four cases, except for the combination of high rotational velocity and low temperature ($452.9\nu_c, 0.25T_c$), dash-dotted line. These solutions can be compared to the approximative (LIA) solution found in Eq. (13), Ref. 21, dotted line. The temperatures are approximative values for ^{3}He-B. The Re_α parameters used in the calculations are: $\mathrm{Re}_\alpha = 78.6$ for $0.25T_c$ and $\mathrm{Re}_\alpha = 0.016$ for $0.95T_c$.

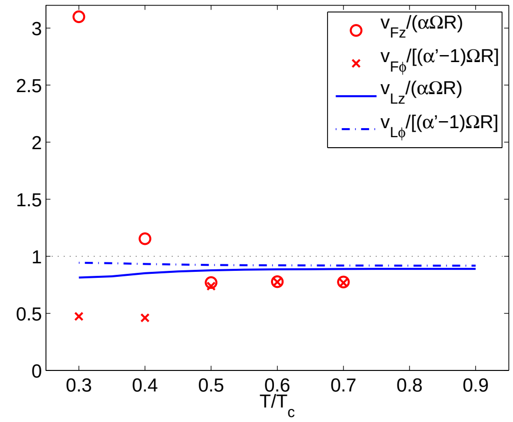

FIG. 7: Comparison of numerically calculated asymptotic velocities between a single vortex end and a vortex front. The lines are for a single vortex, giving the axial (solid line) and azimuthal (dash-dotted line) components. The data points are for the vortex front, giving the axial (circles) and the azimuthal velocity (crosses). All azimuthal velocities are in the rotating coordinate system. The front velocity is from numerical simulations, originally presented in Ref. 4, p. 3219. The parameters are $\nu = 34.0$ and $R/a = 0.88 \times 10^5$.

At high temperatures the axial velocity (Fig. 4b) closely follows the formula in Eq. (11), whereas the azimuthal log-log plot, Fig. 5b, looks linear only when $\ln\nu \gtrsim 3$. Indeed, fitting in the range $\ln\nu \in [3.30, 6.77]$ at $\mathrm{Re}_\alpha = 0.083$ gives $k_\phi = -0.719$ with $\nu_0 \simeq 1.107$.

At low temperatures, the opposite seems to be the case; the axial velocity is nonlinear in the log-log plot (Fig. 4b), while the azimuthal velocity (Fig. 5b) seems to be linear at $\ln\nu \lesssim 4$. Keeping the first point fixed and fitting in the range $\ln\nu \in [\ln\nu_c, 4.00]$ at $\mathrm{Re}_\alpha = 78.6$ ($0.25T_c$ in ^{3}He-B) gives $k_\phi = -0.98$. (Fitting without fixing the first point gives $k_\phi = -0.99$ and $\nu_0 \simeq 1.97$.) At even lower temperatures the vortices converge very slowly to the asymptotic form, so it is difficult to say what the behavior is like at $T = 0$.

The shape of the top part of a rotating vortex is depicted in Fig. 6. The asymptotic form depends somewhat on the parameters. We see that the shape at the critical value $\nu = \nu_c$ is independent on temperature. This is natural since the vortex is at rest in the rotating frame and thus the dissipation does not play any role. The azimuthal angle of the vortices seems constant both at $\nu = \nu_c$ and at high temperatures. We also compare the shape with the one obtained using a simple model having an analytic solution[21].

We can take the expression (11) as a basis for further analysis, including e.g., the analysis of the axial velocity of a moving vortex front. The comparison to the vortex front is made in Fig. 7. The velocity of a moving front is affected by the twisting of vortices behind the front. An analytic formula has been applied to analyze the effect of this twisting on the front velocity[3,22]. What is studied in this paper could be termed as the single vortex contribution to the vortex front velocity; twisting of vortices adds another contribution, surface friction yet another, and phenomena associated with turbulence (reconnections, Kelvin cascade, vortex tangle diffusion, bound fermion states at vortex core) yet another.

V. STABILITY OF VORTICES IN NON-TILTED CYLINDER

A. Our definition of stability

We now consider the stability of vortices in a non-tilted cylinder. From the standpoint of this paper, stability means that the vortex configuration has an asymptotic state with a single vortex, moving upwards and rotating with a constant angular velocity without changing its shape. In order to reach this kind of asymptotic vortex configuration, the angular velocity Ω must be above some critical value Ω_c. Otherwise, the vortex will shrink, and eventually disappear.

B. Critical angular velocity

The critical angular velocity Ω_c depends on the cylinder radius R. The necessity of the critical value can be heuristically justified by recalling that vortex rings need a sufficiently large counterflow being pushed through them in order to grow, and furthermore, realizing that the same is true for vortices that end on walls: counterflow needs to be pushed through the area delimited by the vortex line and the walls. The counterflow in this case is provided by the rotation of the vessel. Without a numerical solution, this idea only provides a rough approximation of the value of Ω_c.

An exact value for Ω_c, however, can be obtained by studying the free energy[23]

$$F = E_{\mathrm{kin}} - \Omega L, \tag{14}$$

where E_{kin} is the kinetic energy and L is the angular momentum of the fluid. In order for a one-vortex state to be stable, F should be smaller for one axial vortex than for the stationary superfluid. This gives the condition

$$\frac{\kappa}{4\pi}\ln\frac{R}{a} - \frac{1}{2}\Omega(R^2 - a^2) \leq 0. \tag{15}$$

We neglect the small term $\propto a^2$. Thus for the one-vortex state to be stable, Ω has to be larger than

$$\Omega_c = \frac{\kappa}{2\pi R^2}\ln\frac{R}{a}. \tag{16}$$

In dimensionless form this can be written $\nu_c \equiv \Omega_c R^2/\kappa = (1/2\pi)\ln(R/a)$.

C. Other causes for instability

Our numerical calculations indicate that once we have a vortex, whose end moves upwards, it is found to be stable at all temperatures, even at the zero temperature limit. Instability is found only if the angular velocity is below the critical value Ω_c, or if the cylinder is tilted. This is somewhat surprising, since previous simulations and experimental studies in ^{3}He-B have indicated that below a certain temperature, roughly $0.5T_c$ (or $\mathrm{Re}_\alpha \gtrsim 1.5$), single vortices become unstable[2,11,14]. We suggest that this kind of single vortex instability is due to some surface effects, or heat leaks causing extra counterflow. In our model, it is assumed that the surface of the cylinder is smooth and that there is no surface-induced extra friction at the vortex end.

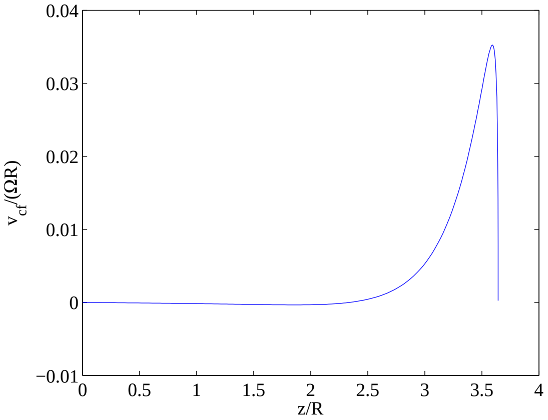

FIG. 8: Value of counterflow projected on the vortex tangent, non-tilted cylinder. There is a clear peak near the top of the vortex, then a rapid drop to zero. The critical value of projected counterflow velocity for Kelvin waves with wavelength R is $v_{c,\mathrm{OG}} = 0.1634\,\Omega R$, which is clearly not reached. The parameters are the same as for the last vortex state in Fig. 2a.

Another source of instability is related to the creation and growth of Kelvin waves. The so-called Ostermeier-Glaberson instability[24,25] appears when the counterflow $\mathbf{v}_{\mathrm{cf}} := \mathbf{v}_{\mathrm{n}} - \mathbf{v}_{\mathrm{s}}$ along the vortex line is sufficiently strong, and causes straight vortex lines to become unstable towards the appearance of Kelvin waves. For a single axially oriented straight vortex, the critical counterflow velocity above which the amplitude of Kelvin waves with a wave vector k are able to grow is:

$$v_{c,\mathrm{OG}} = \frac{\Omega + \eta k^2}{k}, \text{ where } \eta = \frac{\kappa}{4\pi}\ln\frac{1}{ka}. \tag{17}$$

In our case of a non-tilted cylinder with a vortex attached to the cylinder wall this effect may exist in some situations. From Fig. 2b one observes that the vortex has a small component along the azimuthal direction. This results in a non-zero counterflow along the vortex and could in principle cause Ostermeier-Glaberson instability. However, the numerics indicate that the Kelvin waves that could grow have a wavelength much longer than the cylinder radius (and therefore larger than the region of this finite counterflow). Hence, the Kelvin waves cannot grow and Ostermeier-Glaberson instability does not play any role. There is in principle room for Kelvin waves to grow along the lower part of the vortex as well, but since the Kelvin waves that are created in the untilted case move upwards along the vortex line, and since the counterflow along the vortex line has its maximum in the top part of the vortex and falls sharply below it (Fig. 8), there is no chance for Kelvin waves to grow in the lower parts of the vortex either. However, the situation in a tilted rotating cylinder is different. With enough tilting, the boundary superfluid

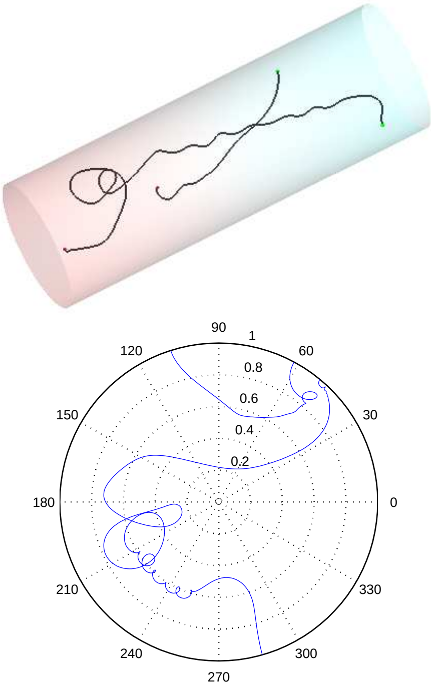

FIG. 9: Kelvin waves created in a rotating tilted cylinder. The appearance of Kelvin waves, (which can be clearly seen in the lower left quadrant of the polar plot) is due to Ostermeier-Glaberson instability caused by the background velocity field $\mathbf{v}_\mathrm{b}$. This background velocity field is nonzero in a rotating tilted cylinder and in this case causes a sufficiently strong counterflow along the vortex line to create Kelvin waves. The parameters are $\alpha\Omega t = 0.56$, $\mathrm{Re}_\alpha = 20.6$ ($\sim 0.3T_c$ in ^{3}He-B), $\Omega R^2/\kappa = 13.6$ and $\theta = 60°$.

velocity $\mathbf{v}_\mathrm{b}$ creates a sufficiently strong counterflow, which results in the appearance of Kelvin waves. These Kelvin waves then produce a change from a laminar to a more turbulent fluid motion, possibly resulting in a vortex tangle, see Fig. 9. Yet another phenomenon is the Crow instability[26] which applies to vortices that are close to each other, or close to the wall (which can be interpreted as close to the image vortex). This instability is due to the fact that vortices of opposite direction attract each other. Thus, the parts of vortices that are slightly closer to each other start moving faster towards each other, deforming the vortices even more, and eventually resulting in a large number of reconnections and new vortices. In our case the Crow instability does not work in the untilted cylinder since the rotation provides a stabilizing effect.

These various causes of instability notwithstanding, we have some doubts about the equations for vortices in a rotating container used in Refs. 11–13. According to our calculations the creation of turbulent states is more difficult than the results in those papers would suggest.

D. Effects of initial vortex state

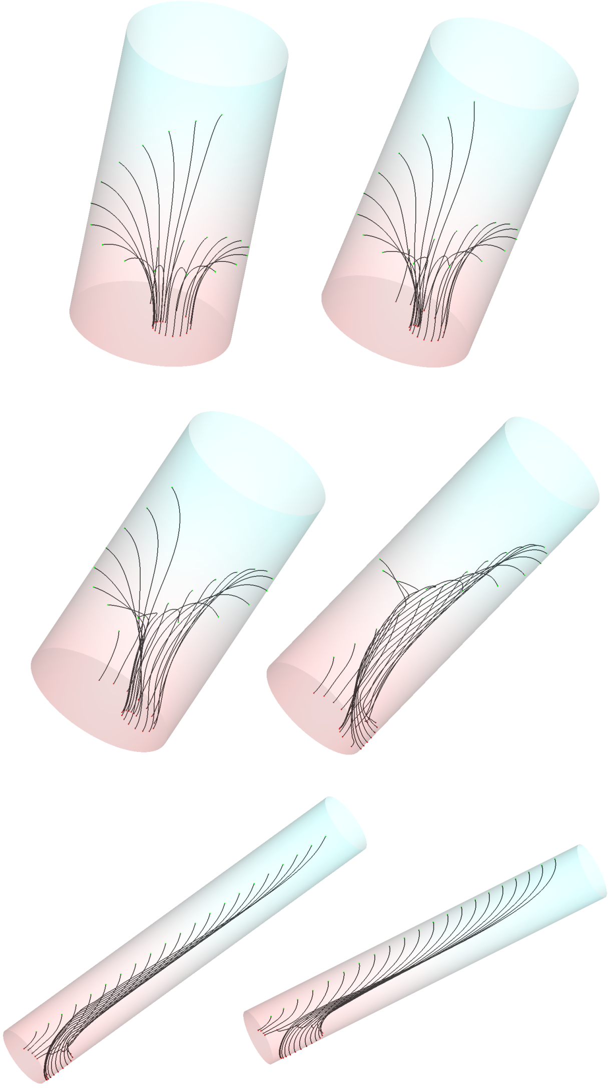

FIG. 10: Vortex evolution for different tilting angles. Twenty-one snapshots are shown for each tilting with angles $\theta = 10°$, $20°$, $30°$, $40°$, $50°$, and $60°$. With increasing tilting some qualitative differences appear. The starting point of the vortex may climb on the side wall. The end point may start moving axially. All plots are in the rotating coordinate system. The total time is $2.33/\alpha\Omega$, $\mathrm{Re}_\alpha = 3.63$ and $\nu = 13.6$.

While it is virtually impossible to carry out an exhaustive study for this case, since the possible space of initial conditions has an infinite-dimensional parameter space, some things can still be said.

The initial vortex state used here was a quarter ring attached at the bottom and at the side wall. This was sufficient to guarantee the required asymptotic state. Before the vortex assumed a behavior close the asymptotic one, there were some transient effects. The velocity of v_{Lz} oscillated before reaching the asymptotic value. This oscillation was stronger at low T/T_c. Furthermore, if the initial radius was large, this oscillation was usually stronger. This can be explained as follows: At small scales, the fluid can always be considered as a bulk fluid having uniform normal and superfluid velocities. For these uniform velocities, the non-oscillating shape for a closed vortex is a perfectly circular ring. Also, at small distances, the curvature of the walls can be neglected, and the shape of the vortex near the wall is the same as in the bulk. Thus, an initial quarter ring vortex with a radius small compared to the cylinder radius is closer to the non-oscillating configuration than a quarter ring vortex with a radius comparable to the cylinder radius.

VI. EFFECT OF TILTING

Tilting the vessel has the advantage of breaking the cylindrical symmetry. A small tilt may be useful in calculations also for detecting effects that occur due to this asymmetry, unavoidably present in experimental situations.

The most noticeable effect of tilting is the oscillation of v_{Lz} about a constant value (close to $\alpha\Omega R$). This is due to a sinusoidal component of the boundary field[16].

A somewhat surprising effect was also found. At a large enough tilt angle the azimuthal velocity of the vortex end may approach to zero (in moving coordinates). Thus, in the asymptotic limit, the vortex end becomes locked at some azimuthal angle, while a constant axial velocity component remains. A detailed study of this phenomenon has not been done yet, but this sort of behavior can be seen in the last two pictures of Fig. 10, corresponding to tilting angles 50° and 60°.

VII. CONCLUSIONS

While one could say that we have been “hitting a mosquito with a cannonball”, using a code created for brute force large scale vortex tangle calculations to do a very simple job, there still is some potentially useful information to be gained from this endeavor.

Vortex motion was found to be quite stable in both the untilted and moderately tilted ($\lesssim 30^\circ$) cases. This limits the causes for the experimentally observed single vortex instability[2,11,14] to areas not covered in this study, such as surface effects and dissipative bulk effects.

The asymptotic line velocities $\alpha\Omega R$ and $(\alpha' - 1)\Omega R$, valid in the $\Omega R^2/\kappa \gg 1$ limit for the untilted case, could be generalized by equations of type (11) with some yet unexplained numerical constants. Providing an explanation for these constants might necessitate analyzing, either analytically or numerically, the shape of the vortex, or including varying also the parameter R/a.

This study also highlights the role of scaling properties in superfluids and other analogous systems. A deeper analysis to connect these formulas to the velocity of the vortex front should be carried out. The azimuthally locked motion in the tilted case was an unexpected result.

Acknowledgments

This work is supported by the Academy of Finland and EU 7th Framework Programme (FP7/2007-2013, grant 228464 Microkelvin).

---

[1] W. F. Vinen and J. J. Niemela, J. Low Temp Phys. **128**, 167 (2002).
[2] V. Eltsov et al., in *Progress in Low Temperature Physics: Quantum Turbulence*, edited by W. B. Halperin and M. Tsubota (Elsevier, 2009), vol. 16, chap. 2, pp. 45–146.
[3] V. B. Eltsov et al., Phys. Rev. Lett. **96**, 215302 (2006).
[4] A. P. Finne et al., Rep. Prog. Phys. **69**, 3157 (2006).
[5] C. F. Barenghi, R. J. Donnelly, and W. F. Vinen, eds., *Quantized Vortex Dynamics and Superfluid Turbulence* (Springer, 2001).
[6] K. W. Schwarz, Phys. Rev. B **31**, 5782 (1985).
[7] R. Hänninen, A. Mitani, and M. Tsubota, J. Low Temp Phys. **138**, 589 (2005).
[8] R. Hänninen et al., J. Low. Temp. Phys. **155**, 98 (2009).
[9] R. J. Zieve et al., Phys. Rev. Lett. **68**, 1327 (1992).
[10] K. W. Schwarz, Phys. Rev. B **47**, 12030 (1993).
[11] A. P. Finne et al., Nature **424**, 1022 (2003).
[12] M. Tsubota, T. Araki, and C. F. Barenghi, Phys. Rev. Lett. **90**, 205301 (2003).
[13] M. Tsubota, C. F. Barenghi, T. Araki, and A. Mitani, Phys. Rev. B **69**, 134515 (2004).
[14] A. P. Finne et al., Phys. Rev. Lett. **96**, 085301 (2006).
[15] E. B. Sonin, Rev. Mod. Phys. **59**, 87 (1987).
[16] R. Hänninen, J. Low. Temp. Phys. **156**, 145 (2009).
[17] T. D. C. Bevan et al., J. Low. Temp. Phys. **109**, 423 (1997).
[18] H. E. Hall, J. Phys.: Condens. Matter **11**, 7677 (1999).
[19] C. E. Swanson and R. J. Donnelly, J. Low. Temp. Phys. **61**, 363 (1985).
[20] K. W. Schwarz, Phys. Rev. B **38**, 2398 (1988).
[21] E. B. Sonin and S. K. Nemirovskii, Phys. Rev. B **84**, 054506 (2011).
[22] V. Eltsov et al., J. Low Temp. Phys. **150**, 373 (2008).
[23] L. J. Campbell and R. M. Ziff, Phys. Rev. B **20**, 1886 (1979).
[24] W. I. Glaberson, W. W. Johnson, and R. M. Ostermeier, Phys. Rev. Lett. **33**, 1197 (1974).
[25] R. M. Ostermeier and W. I. Glaberson, J. Low Temp. Phys. **21**, 191 (1975).
[26] S. C. Crow, AIAA Journal **8**, 2172 (1970).
[27] If R is increased and Ω is kept constant, the maximum counterflow velocity ΩR may exceed some critical velocity v_c and cause the analysis to become unphysical. We can avoid this by setting $\Omega = \gamma v_c/R$, where γ is some constant, $0 < \gamma < 1$. Then the condition $\Omega R^2/\kappa \gg 1$ will be satisfied, when $\gamma v_c R/\kappa \gg 1$. This proves that the limiting case above is not physically unreasonable, i.e. that it can in principle be approached in experiments.